Proceedings of the 7th International Conference on HydroScience and Engineering

Philadelphia, USA September 10-13, 2006 (ICHE 2006)

ISBN: 0977447405

Drexel University

College of Engineering

A NEW APPROACH FOR IMPLEMENTING THE HLL APPROXIMATE RIEMANN SOLVER FOR ONE-DIMENSIONAL DAM-BREAK FLOWS

Xinya Ying[1] and Sam S. Y. Wang[2]

ABSTRACT

Several new techniques are proposed to overcome the deficiencies in the conventional formulation of the approximate Riemann solvers for one-dimensional dam-break flows, which include numerical imbalance and failure to satisfy mass conservation. The former arises in the case of irregular geometry and the latter in the presence of a hydraulic jump. These new techniques include: (1) adopting the form of the Saint Venant equations which include only one source term representing driving forces; (2) using water surface level as one of the primitive variables, in stead of cross-sectional area; (3) defining discharge at interface and evaluating it according to the flux obtained by the HLL Riemann solver (Harten et al 1983). The performance of the resulting schemes is evaluated by means of theoretical analysis and various test examples, including ideal dam-break flows with dry bed, hydraulic jump, steady flow over bump with hydraulic jump, and a real-life dam-break flow in natural river valley with complex geometry. It is demonstrated that the scheme has excellent numerical balance and mass conservation property and is capable of satisfactorily reproducing various complicated open channel flows.

1. INTRODUCTION

Modeling open channel flows with discontinuities, mixed flow regimes, and irregular geometry has been a great challenge to hydraulic researchers and engineers. Recently, the applications of TVD schemes and approximate Riemann solvers to one-dimensional open channel flows were frequently reported (e.g., Garcia-Navarro and Vazquez-Cendon, 2000; Sanders, 2001; Delis, 2002). These schemes were originally developed to deal with gas dynamics problems. They are accurate in some situations, but the problems such as numerical imbalance and failure to satisfy mass conservation arise when the channel has complex geometry and the flow includes a hydraulic jump. In conventional formulation, the momentum equation includes three terms that respectively represent the hydrostatic pressure force, the pressure force due to cross-sectional variations, and the gravity effect due to bed slope. The numerical imbalance is created when these terms are calculated using different methods, which leads a numerical flow even in a still water test case. On the other hand, Delis (2002) evaluated Roe's Riemann solver and several TVD schemes by means of several test

[1]Xinya Ying, Research Assistant Professor, National Center for Computational Hydroscience and Engineering, The University of Mississippi, MS38677, USA (ying@ncche.olemiss.edu)
[2]Sam S. Y. Wang, F.A.P. Barnard Distinguished Professor, National Center for Computational Hydroscience and Engineering, The University of Mississippi, MS38677, USA (wang@ncche.olemiss.edu)

cases with a hydraulic jump and revealed that the solutions can not satisfy mass conservation at the several cells near the hydraulic jump.

This paper presents a new approach for implementing the HLL approximate Riemann solvers for one-dimensional dam-break flows, which is able to overcome the deficiencies in the conventional formulation, such as numerical imbalance and failure to satisfy mass conservation. The performance of the resulting schemes is evaluated using several test examples with analytic solutions or measured data and is compared with a conventional scheme.

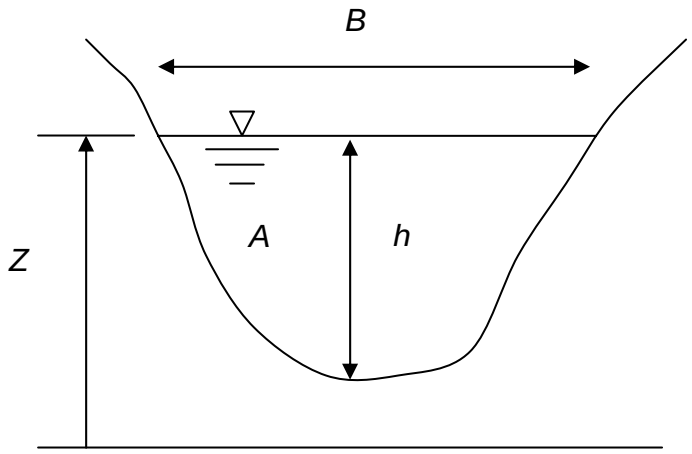

Figure 1 Definition sketch of cross-sectional geometry

2. GOVERNING EQUATIONS

One-dimensional unsteady flows in a natural channel with irregular cross-sections are often described by the Saint Venant equations, that is

$$\mathbf{D}\frac{\partial \mathbf{U}}{\partial t}+\frac{\partial \mathbf{F(U)}}{\partial x}=\mathbf{S(U)} \tag{1}$$

where $\mathbf{D}=\begin{bmatrix} B & 0 \\ 0 & 1 \end{bmatrix}$, B = channel width at water surface elevation (see Figure 1); **U, F(U),** and **S(U)** are respectively the vectors of primitive variables, fluxes, and sources, defined as follows.

$$\mathbf{U}=\begin{bmatrix} Z \\ Q \end{bmatrix} \qquad \mathbf{F(U)}=\begin{bmatrix} Q \\ \dfrac{Q^2}{A} \end{bmatrix} \qquad \mathbf{S(U)}=\begin{bmatrix} 0 \\ -gA\dfrac{\partial Z}{\partial x}-g\dfrac{n^2 Q|Q|}{R^{4/3}A} \end{bmatrix}$$

In above equations, Z = water surface level; Q = discharge; A = cross-sectional area; g = gravitational acceleration; n = Manning's coefficient; and R = hydraulic radius (=A/P); P = wetted perimeter of the channel.

The above form of the Saint Venant equations is commonly used in engineering practice (e.g., Chow, 1959; Cunge et al., 1980; Graf and Altinakar, 1998; Ying et al., 2004). Note that the term $B\dfrac{\partial Z}{\partial t}$ in the continuity equation is equals to $\dfrac{\partial A}{\partial t}$. In the equation, the driving forces are represented

by only one term with the water surface gradient, which makes it very nice for treating the source term because: (1) the variation of water surface is generally much smoother than water depth and bottom; (2) it eliminates the problems such as numerical imbalance that arises due to using different methods to discretize source terms. As a matter of fact, Nujic (1995) proposed a balancing technique in which the pressure term due to water depth is extracted from the flux and combined into the bottom slope term, which actually resulted in a similar form of the governing equation as Eq. (1). In addition, it should be pointed out that the adoption of Eq. (1) as the governing equation automatically incorporates the SGM (Surface Gradient Method) balancing technique (Zhou et al., 2001) into the model formulation.

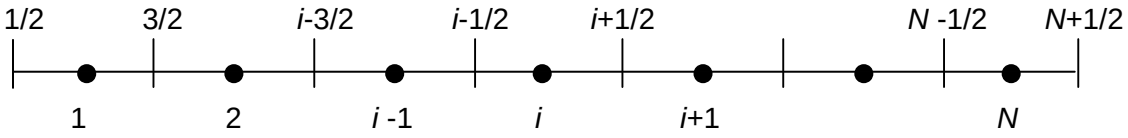

Figure 2 Definition sketch of computational grid

3. NUMERICAL SCHEME

The finite volume method is employed for solving the governing equations. Fig. 2 shows the computational grid, which has *N* cells, *N-1* interfaces between cells and two boundary interfaces.

Integrating Eq. (1) over the i^{th} cell with length of Δx_i yields

$$\mathbf{D}_i \frac{\partial}{\partial t}\int_{\Delta x_i} \mathbf{U}dx + \int_{\Delta x_i} \frac{\partial \mathbf{F(U)}}{\partial x}dx = \int_{\Delta x_i} \mathbf{S(U)}dx \tag{2}$$

where $\mathbf{D}_i$ represents the mean values of **D** over the entire i^{th} cell.

Applying Green's theorem to Eq. (2) and using explicit scheme for time advancing, the following discretized equation is obtained.

$$\mathbf{U}_i^{n+1} = \mathbf{U}_i^n - \frac{\Delta t}{\Delta x_i}\mathbf{D}_i^{-1}\left(\mathbf{F}_{i+1/2} - \mathbf{F}_{i-1/2}\right) + \Delta t \mathbf{D}_i^{-1}\mathbf{S}_i \tag{3}$$

where $\mathbf{U}_i$ is the vector of primitive variables at i^{th} cell center, representing the average values over the entire cell; $\mathbf{F}_{i+1/2}$ and $\mathbf{F}_{i\text{-}1/2}$ are the fluxes at $(i+1/2)^{th}$ and $(i\text{-}1/2)^{th}$ interfaces, see Fig. 2.

According to Godunov (1959), the variables are approximated as constant states within each cell and then the fluxes at interfaces are calculated by solving resultant Riemann problems that exit at interfaces. Here the HLL approximate Riemann solver, proposed by Harten, Lax and van Leer (1983), is used to calculate the intercell flux, because of its robustness and ease to implement. The HLL scheme assumes only one constant intermediate state between the left wave and the right wave, as shown in Fig.3. The intercell flux is defined as

$$\mathbf{F}_{HLL} = \begin{cases} \mathbf{F}_L & \text{when } S_L \geq 0 \\ \mathbf{F}^* & \text{when } S_L < 0 < S_R \\ \mathbf{F}_R & \text{when } S_R \leq 0 \end{cases} \tag{4}$$

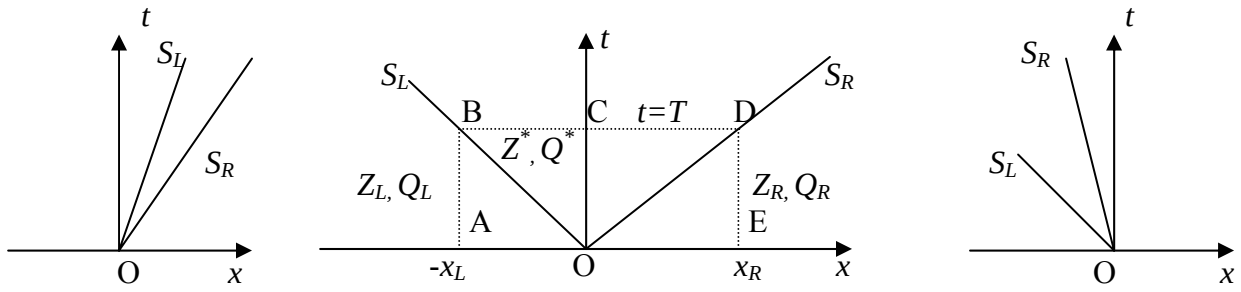

(a) (b) (c)

Figure 3 Three possible wave configurations

where S_L and S_R are left and right wave speeds, respectively, see Fig.3. That is, the flux at an interface is determined by the left state if $S_L \geq 0$ (Fig. 3-a), and by the right state if $S_R \leq 0$ (Fig. 3-c). When $S_L < 0$ and $S_R > 0$ (Fig. 3-b), the flux $\mathbf{F}^*$ is determined by the conservation laws and the assumption that channel is locally prismatic in each cell. Let f_1^* and f_2^* are two components of the flux $\mathbf{F}^*$, that is, $\mathbf{F}^* = \left[f_1^*, f_2^*\right]^T$. Applying the mass conservation law on the control volume OABC and OCDE (see Fig. 3-b), we can obtain

$$f_1^* = \frac{S_R B_R f_1^L - S_L B_L f_1^R + S_L B_L S_R B_R (Z_R - Z_L)}{S_R B_R - S_L B_L} \tag{5}$$

Applying the momentum conservation law on the control volume OABC and OCDE, respectively, we can obtain

$$f_2^* = \frac{S_R f_2^L - S_L f_2^R + S_L S_R (Q_R - Q_L)}{S_R - S_L} \tag{6}$$

The wave speeds S_L and S_R are estimated according to the following equations.

$$S_L = \min\left(V_L - \sqrt{g\bar{h}_L}, V^* - \sqrt{g\bar{h}^*}\right) \tag{7}$$

$$S_R = \max\left(V_R + \sqrt{g\bar{h}_R}, V^* + \sqrt{g\bar{h}^*}\right) \tag{8}$$

where V_L and V_R are velocities of the left and right states, respectively; $\bar{h}_L$ and $\bar{h}_R$ are averaged water depth of the left and right states, which is defined according to $\bar{h} = A/B$.

$$V^* = \frac{1}{2}(V_L + V_R) + \sqrt{g\bar{h}_L} - \sqrt{g\bar{h}_R} \tag{9}$$

$$\sqrt{gh^*} = \frac{1}{2}\left(\sqrt{g\bar{h}_L} + \sqrt{g\bar{h}_R}\right) + \frac{1}{4}(V_L - V_R) \tag{10}$$

Note that for a dry bed problem the wave speeds S_L and S_R are estimated according to the following expressions.

$$S_L = V_L - \sqrt{g\bar{h}_L}\ , \quad S_R = V_L + 2\sqrt{g\bar{h}_L} \qquad \text{for right dry bed} \qquad (11)$$

$$S_L = V_R - 2\sqrt{g\bar{h}_R}\ , \quad S_R = V_R + \sqrt{g\bar{h}_R} \qquad \text{for left dry bed} \qquad (12)$$

The HLL approximate Riemann solver discussed above is a first-order scheme. The second-order spatial accuracy can be obtained through a piecewise linear reconstruction of primitive variables in each cell, which leads to

$$\mathbf{U}^L_{i+\frac{1}{2}} = \mathbf{U}_i + \frac{\Delta x_i}{2}\left(\frac{\partial \mathbf{U}}{\partial x}\right)_i \qquad (13)$$

$$\mathbf{U}^R_{i+\frac{1}{2}} = \mathbf{U}_{i+1} - \frac{\Delta x_{i+1}}{2}\left(\frac{\partial \mathbf{U}}{\partial x}\right)_{i+1} \qquad (14)$$

In order to avoid numerical oscillations, proper slope limiters must be used in estimating the slope $\frac{\partial \mathbf{U}}{\partial x}$. Here, the minmod limiter is adopted due to its robustness. Therefore, the slope in the i^{th} cell can be expressed as

$$\left(\frac{\partial \mathbf{U}}{\partial x}\right)_i = \text{minmod}\left(\frac{\mathbf{U}_i - \mathbf{U}_{i-1}}{x_i - x_{i-1}}, \frac{\mathbf{U}_{i+1} - \mathbf{U}_i}{x_{i+1} - x_i}\right) \qquad (15)$$

The minmod function is defined as the argument with smaller value if all arguments have the same sign and otherwise it is zero.

The source terms in Eq. (3) include the water surface gradient term and the friction term. The water surface gradient is computed by centered difference approach. The friction term is explicitly evaluated based on the pointwise method. Therefore, the values of Z and Q at next time can be obtained by solving Eq. (3) explicitly. Such a method is often referred to as the cell centered scheme as both variables Z and Q are defined at cell centers. For convenience, hereafter this scheme is referred as the HLL-A scheme. However, the solution of the discharge from such a numerical scheme may not satisfy mass conservation law in the event that there is a hydraulic jump, as shown in the numerical tests that follow.

To find a solution to this problem, let us first look at the discretized equation (3). For clarity, the continuity equation in Eq.(3) is rewritten as

$$Z_i^{n+1} = Z_i^n - \frac{1}{B_i}\frac{\Delta t}{\Delta x_i}\left[\left(f_1\right)_{i+1/2} - \left(f_1\right)_{i-1/2}\right] \qquad (16)$$

It is important to note that in the discretized continuity equation, the variable Q is replaced by the flux f_1. Therefore, it is obvious that the continuity equation only ensure the conservation property of the flux f_1, instead of discharge Q. Let us take a steady flow as an example. When the solution converges at steady state, i.e. $Z_i^{n+1} = Z_i^n$, from the continuity equation (16), we can see that the flux f_1 has the same value at all interfaces, which is equal to the inflow discharge or the flux f_1 at inflow boundary. In other words, the flux f_1 has the exact conservation property, while the discharge Q calculated by the momentum equation is not ensured to have such property. For this reason, we choose the values of flux f_1 as the solution of discharge, while the values of Q_i

calculated by Eq. (3) are only used to define the constant states of the Riemann problems. The resulting scheme is called the HLL-B scheme.

The solution procedures for the proposed schemes are summarized below:

(1) Performing piecewise linear reconstruction of primitive variables in each cell according to Eqs. (13), (14), and (15). Note that this step is required only for the second-order scheme;

(2) Calculating wave speeds according to Eqs. (7) and (8) or Eqs. (11) and (12);

(3) Evaluating fluxes by Eqs. (4), (5) and (6). For the HLL-B scheme, discharge Q is evaluated based on $Q = f_1^*$;

(4) Obtaining the values of Z and Q at cell centers at next time from Eq. (3). For the HLL-A scheme, these values are considered as the solutions of Z and Q. For the HLL-B scheme, only the values of Z are used as the solution, while the values of Q are provisional and only used to define the Riemann problems at next time.

It should be noted that the solution procedures for both HLL-A and HLL-B schemes are essentially identical. The only difference between two schemes is the approaches used to evaluate discharges. In the HLL-A scheme, discharges are estimated in conventional way, that is, according to the momentum equation, while in the HLL-B scheme discharges are assumed to be equal to the values of flux f_1. For this reason, the both schemes give the same results of water level Z.

It is easy to see that the resulting schemes do not cause numerically generated flow or numerical imbalance problem. Let us consider an open channel filled with water at rest. Obviously, the water will remain at rest if no disturbance is applied to the domain and boundaries. If we apply above schemes to simulate this case, we can see the source terms, including water surface gradient term and friction term, and flux terms in Eq. (3) are exactly equal to zero at initial time, no matter how bottom and cross-section change. As a result, the solutions of Z and Q at succeeding time will remain the same as initial state, in other words, no flow is numerically generated.

Like most explicit schemes, the schemes discussed above are subject to the Courant-Friedrichs-Lewy stability condition, that is

$$N_{CFL} = \mathrm{Max}\left[\frac{\Delta t}{\Delta x_i}(|V_i| + \sqrt{gA_i / B_i})\right] \le 1 \qquad (1 \le i \le N) \tag{17}$$

4. BOUNDARY CONDITIONS AND DRY BED TREATMENT

For control volume method, boundary conditions are often treated by introducing ghost cells. In these ghost cells, primitive variables and their gradients are specified. In the event that inflow is subcritical, discharge is often specified at the ghost cell and water level is evaluated by extrapolation based on the values of two adjacent interior cells. For supercritical inflow, both discharge and water level are specified at the ghost cell and gradient of water level is set to zero. At open outflow boundary, both discharge and water level at the ghost cell are calculated by linear extrapolation based on the values of two adjacent interior cells. For the outflow boundary with specified water level, the water level at the ghost cell is set to the specified value. This approach to treat boundary conditions is common and often sufficient for control volume method (Sanders, 2001).

Channel flows may occur over initially dry areas. The commonly used approach to deal with this problem is to define a sufficiently small water depth and zero velocity at dry nodes, so that the dry domain can be computed in the same way as wet part without introducing significant error.

5. NUMERICAL TESTS

5.1 Idealized dam-break problem in a rectangular channel with dry bed

Consider a 1200 m long channel with rectangular cross-section, which is assumed to be horizontal and frictionless. A dam is located at 500 m from upstream end of the channel. Initially, upstream water depth is 10 m and downstream channel is dry. This is an ideal dam-break example and has been widely used for testing numerical schemes (e.g., Zoppou and Roberts, 2003; Ying et al., 2004). In the computation, Δx = 10 m, Δt = 0.1 s, and initial water depth in the downstream channel was specified as 10-40 m.

The numerical and exact solutions of water depth *h*, discharge *Q*, and velocity *V* at 30 s after the dam failure are presented in Figs.4 (a), (b) and (c), respectively. The exact solutions can be found in the books by Toro (2001) and Graf and Altinakar (1998). Note that the HLL-A scheme results in the same results as the HLL-B scheme for this example in terms of water depth *h*, discharge *Q*, and velocity *V*. Therefore, in Fig.4 only results from the HLL-B schemes are presented. Fig.4 shows that both the first-order and the second-order schemes result in overall reasonable solutions, which have no entropy violation. As expected, the first-order scheme is more diffusive that the second-order scheme.

Fig. 4(c) reveals that the solutions of velocity are evidently under-predicted near the wave front edge. In fact, most of numerical schemes have difficulties to accurately predict velocity near the wave front edge for dry bed dam-break problem, because of very small water depth in the area. For example, Sanders (2001) reported that the Roe-type Riemann solver with MUSCL approach predicted velocity with significant under-prediction or over-prediction near the front edge, which is strongly dependent on the selection of N_{CFL}. It should be noted that this insufficiency only results in very limited influence on the flow, which can be observed from the numerical solutions of water depth and discharge, as shown in Figs. 4(a) and (b) respectively. Further tests demonstrate that the solutions by the present schemes are almost independent of N_{CFL}, that is, no significant difference in solutions is observed by using different time step as long as N_{CFL} is kept less than one.

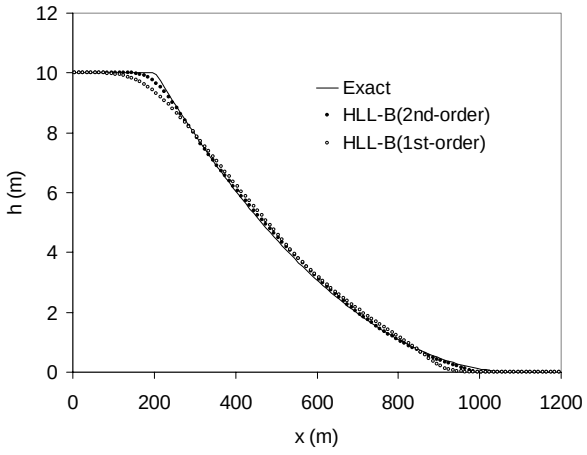

(a) water depth

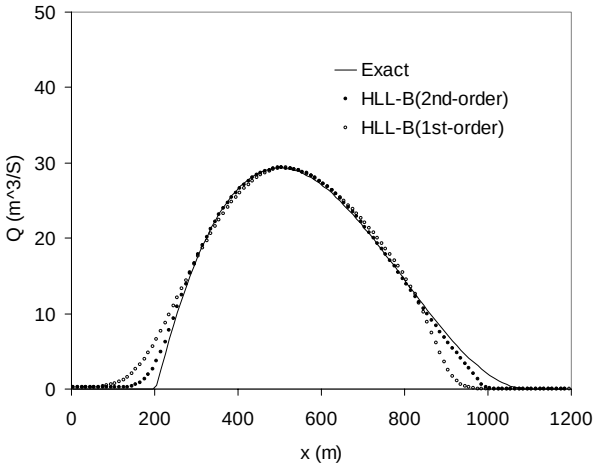

(b) discharge

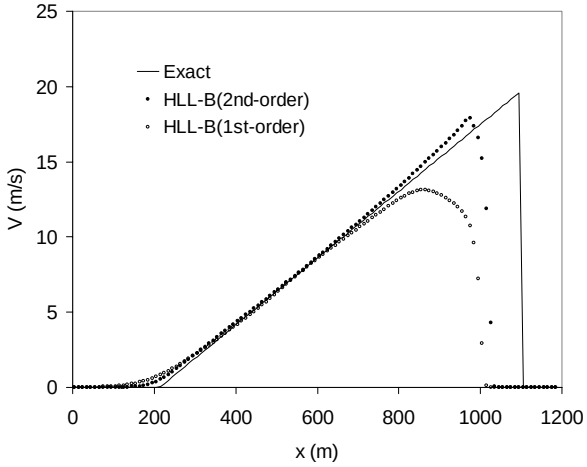

(c) velocity

Fig. 4 Numerical solutions of dam-break problem in a rectangular channel with dry bed at t = 30 s

5.2 Hydraulic jump in a rectangular channel

This test case is selected to demonstrate that the proposed scheme can satisfactorily reproduce not only the location and height of a hydraulic jump, but also the discharges along the channel. The computed results are verified against the experimental data measured in a 14.0 m long and 0.46 m wide metal flume with horizontal bottom (Gharangik and Chaudhry, 1991). In the experiment, the water depth at the upstream boundary is 0.031 m, velocity is 3.831 m/s, and corresponding Froude number is 7.0. Water depth at downstream end is 0.265 m. In the computation the channel was discretized by 47 cells. The time step was 0.05 s. Initial water depth and velocity over the entire channel was assumed to be the same as those at the upstream boundary. The water depth at the downstream boundary was increased from 0.031 m to 0.265 m in 50 seconds and maintained until a steady hydraulic jump was formed. Value of the Manning's coefficient n = 0.0085 s/m$^{1/3}$ was used, which was determined by matching experimental data with simulation results and is within the range of 0.008 to 0.011, as suggested by the experiment.

Fig. 5(a) shows that the location of the hydraulic jump is predicted by both the first-order and the second-order schemes with satisfactory accuracy. The numerical solutions of discharge along

channel from the HLL-A scheme and the HLL-B scheme are presented in Fig. 5(b). Since it is steady flow, the discharge should keep constant along the entire channel length. From this figure, it is observed that the solutions from the HLL-A schemes do not converge at the exact solution over 2 or 3 cells near the hydraulic jump. In other words, the solutions of discharge do not satisfy the mass conservation law. Such non-conservative solution of the discharge at the location of hydraulic jump is also reported by several researchers in their steady flow over bump test case (e.g., Vazquez-Cendon, 1999; Hubbard and Garcia-Navarro, 2000; Zhou et al., 2001; Rogers et al., 2003). In contrast, the exact conservation property of the HLL-B schemes is observed. The difference between numerical solutions from the HLL-B schemes and the exact value of discharge (=0.0546 m^3/s) along the entire channel length is indistinguishable in the figure.

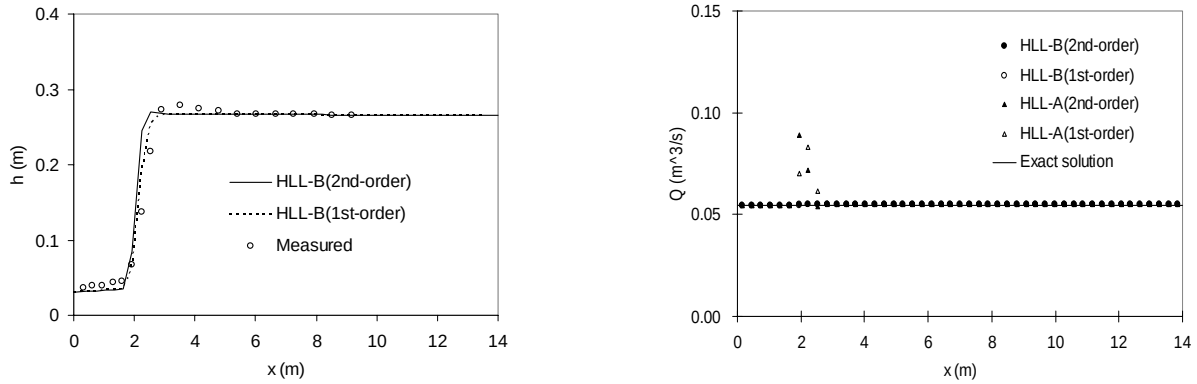

(a) water depth (b) discharge

Fig. 5 Numerical solutions for the hydraulic jump test case in a rectangular channel

5.3 Steady flow over a bump

Consider a 1 m wide and 25 m long channel with rectangular cross-section. The channel bed is assumed to be horizontal and frictionless. Bottom elevation Z_b is defined by

$$Z_b = \begin{cases} 0 & x < 8 \text{ and } x > 12 \\ 0.2 - 0.05(x-10)^2 & 8 \le x \le 12 \end{cases} \tag{18}$$

The downstream boundary condition of $Z = 0.33$ m and the inflow condition of $Q = 0.18$ m^3/s were imposed in the computation. This test case was widely used to study the convergence of numerical solution to a steady state and the conservation of discharge along distance (e.g., Vazquez-Cendon, 1999; Zhou et al., 2001; Valiani, 2002)

The analytic solution for this test case was obtained by the Bernoulli equation and the location of hydraulic jump was determined by the conservation of momentum across the jump. In the computation the grid size was the same as used in the numerical simulation by Valiani et al. (2002), that is, Δx =0.1m, so that the computed results from the present scheme can be compared with the existing results from other numerical schemes. The time step Δt = 0.01 was used.

Fig. 6(a) shows that the numerical solution of water level is in good agreement with the analytic solution. Particularly, the location of the hydraulic jump is accurately predicted. Fig. 6(b) indicates that the solution from the HLL-B scheme has excellent conservation property and the

difference between predicted and exact discharge is indistinguishable. In contrast to this, the discharge from the HLL-A schemes does not satisfy the mass conservation law over several cells adjacent to the hydraulic jump, which are similar to those from the HLL approximate Riemann solver with the surface gradient method (Zhou et al., 2001) and the corrected upwind method (Delis, 2003) for the treatment of the source terms.

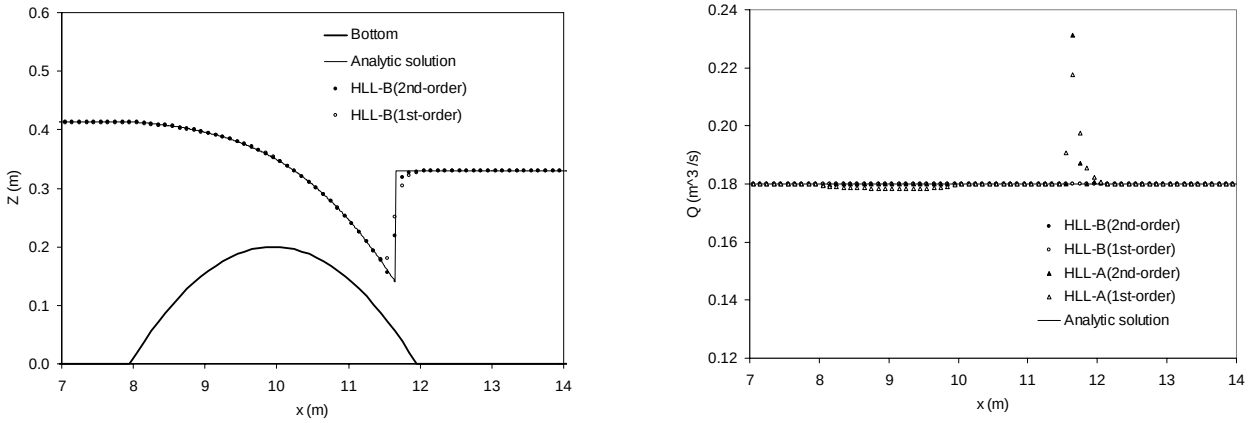

Fig. 6 Numerical solutions for the test case of steady flow over a bump with hydraulic jump

5.4 Propagation of flood wave in the Toce River Valley

This test example, which was used as a benchmark test case in the CADAM project (Soares Frazao et al., 2000), is selected to demonstrate the numerical model's capability to deal with a real-life problem with irregular cross-sections and non-uniform grid. The topography of Toce River is shown in Fig. 7. The computational domain was divided into 61 cells, which was quite non-uniform and the length of cells varied from 0.25 to 1.94 m, as shown in Fig. 8. Fig. 9 shows the discharge-time hydrograph of inflow. A free outflow boundary condition was imposed in the computation. The value of the Manning's coefficient was 0.02 $s/m^{1/3}$, as used in most of previous 1D simulations of the Toce River Test Case (e.g., Soares Frazao and Zech, 1999; Rosu and Ahmed, 1999). The entire domain was assumed to be dry at initial time. In the computation, the initial water depth in the domain was set to 0.01 m. The time step was 0.1 s and the corresponding maximum value of N_{CFL} was 0.7. The total number of time steps was 1800. The computational time was 0.33 s on a PC with AMD Athlon processor (1.46 GHz). The topographic data and inflow discharge hydrograph used in the computation were the same as those in the physical model so that the numerical results can be directly compared with the experimental data.

Computational results of water surface level and discharges at t = 30, 60, and 120 s are presented in Figs. 10 and 11, respectively. These figures give a rough idea about the flood propagation in the river valley. In Fig.10, the variation of water surface level due to uneven topography and formation of hydraulic jumps are observed. The presence of hydraulic jumps can be confirmed from Fig. 12, which displays the Froude Number as a function of distance *x* and clearly reveals that there are several transitions between supercritical flow and subcritical flow. Fig. 11 shows the comparisons of computed discharges between the HLL-A scheme and the HLL-B scheme. It is observed that the HLL-B scheme produces reasonable solutions, whereas the HLL-A scheme fails to correctly predict the discharges at the locations where hydraulic jumps take place, which is similar to those in the aforementioned hydraulic jump and steady flow over bump test cases. To further demonstrate the conservation property of the HLL-B scheme, a steady flow test case is performed in which a constant discharge of 0.1 m^3/s is imposed at the inlet boundary and no

distinguishable difference between predicted discharge and the exact value over the entire domain is observed.

Fig. 13 shows that the computed stage-time hydrographs at four selected observation points from upstream to downstream are in good agreement with the measured data. Note that the numerical result represents the average value over a cross-section, while experimental result represents the value at an observation point. This is a probable cause for the existence of discrepancy between predicted and measured results in certain regions. Fig. 14 shows that the computed results of maximum water level are in reasonable agreement with the measured data from the physical model, except for the observation point P9 where the predicted maximum water level is lower than the measured value because the local water surface rise due to the influence of reservoir embankment can not be correctly reproduced by a one-dimensional model.

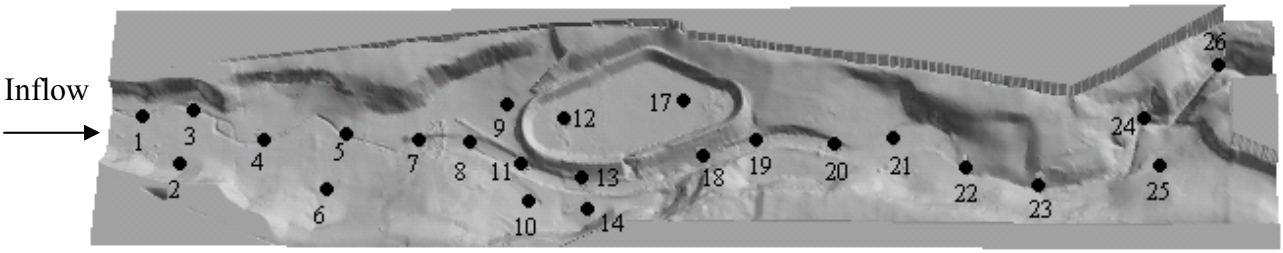

Fig. 7 Topography of the Toce River Valley and locations of measurement points

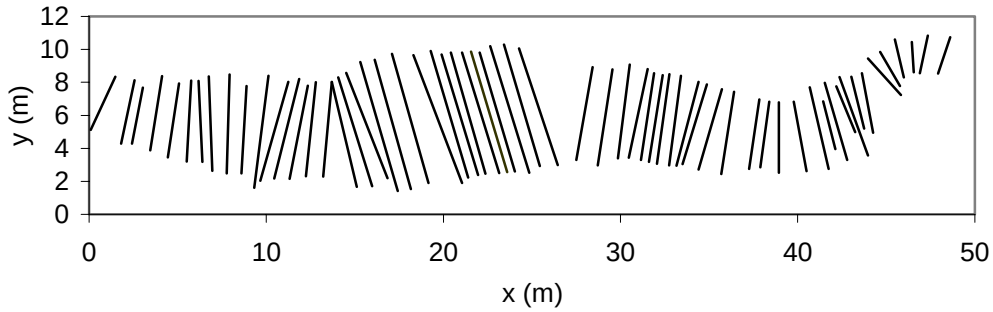

Fig. 8 Locations of computational cross-sections for the Toce River test case

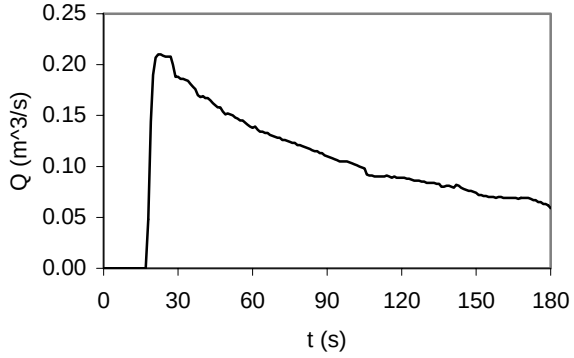

Fig. 9 Discharge-time hydrograph at inflow boundary for the Toce River test case

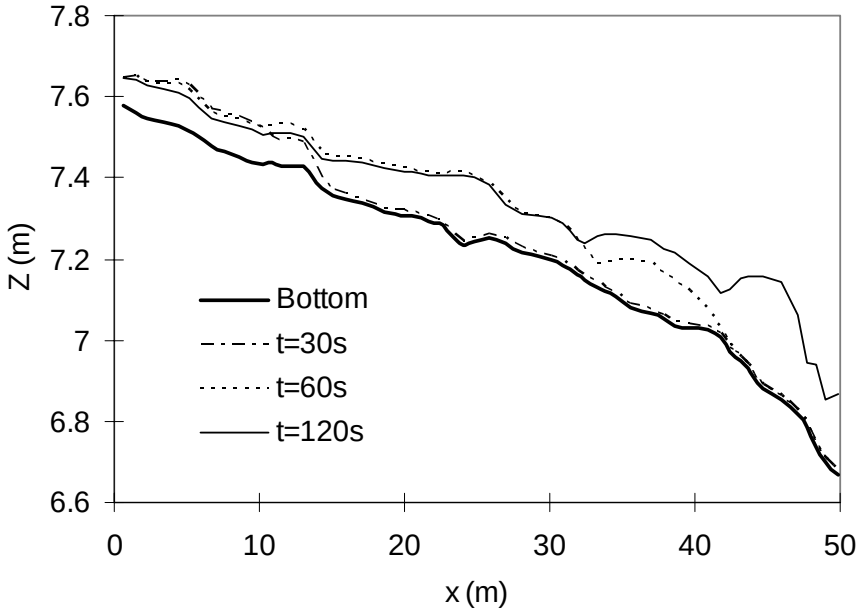

Fig. 10 Computed water surface elevations at t = 30, 60, and 120 s for the Toce River test case

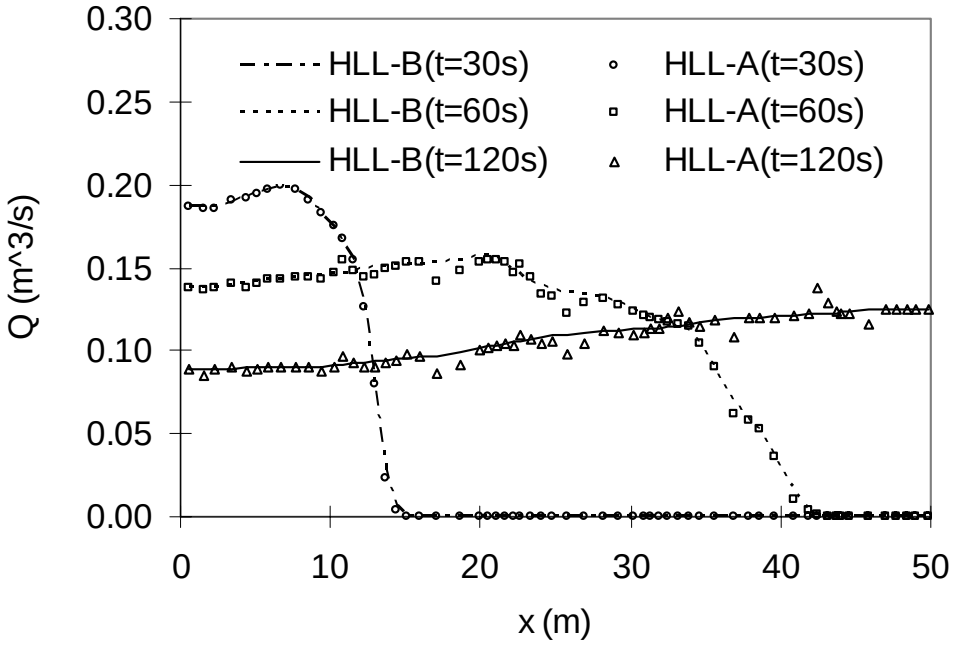

Fig. 11 Computed discharges at t = 30, 60, and 120 s for the Toce River test case

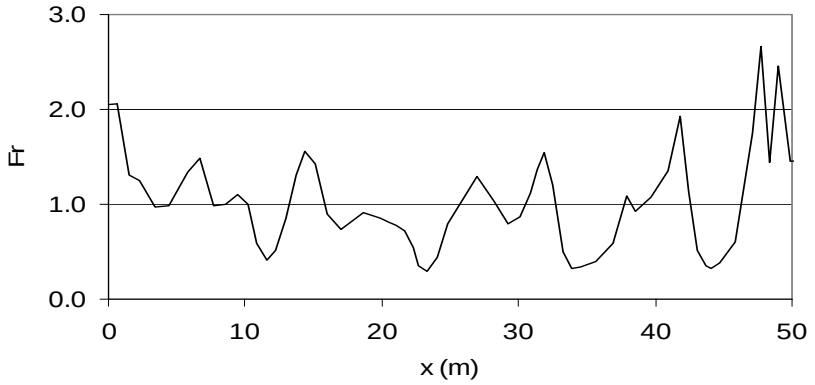

Fig.12 Froude Number *Fr* as a function of *x* at t = 120 s for the Toce River test case

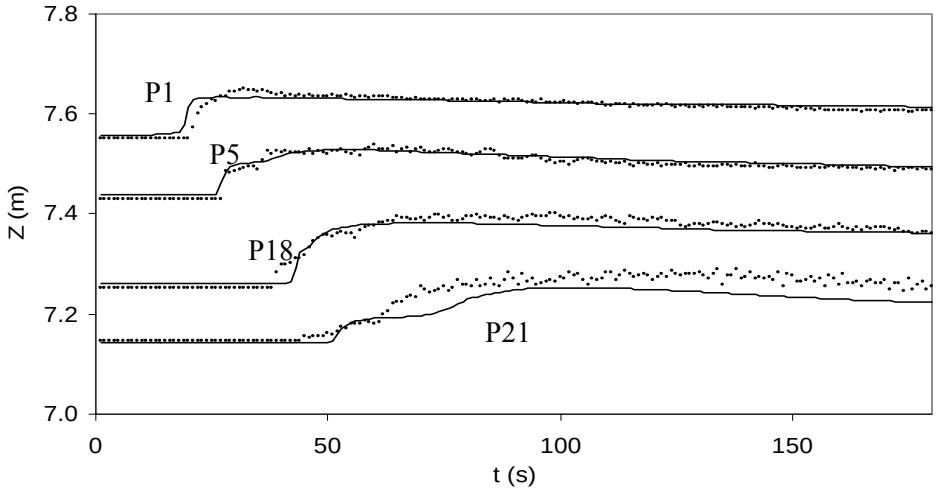

Fig. 13 Comparisons of computed stage-time hydrographs (solid line) with measured data (dot) at four observation points for the Toce River test case

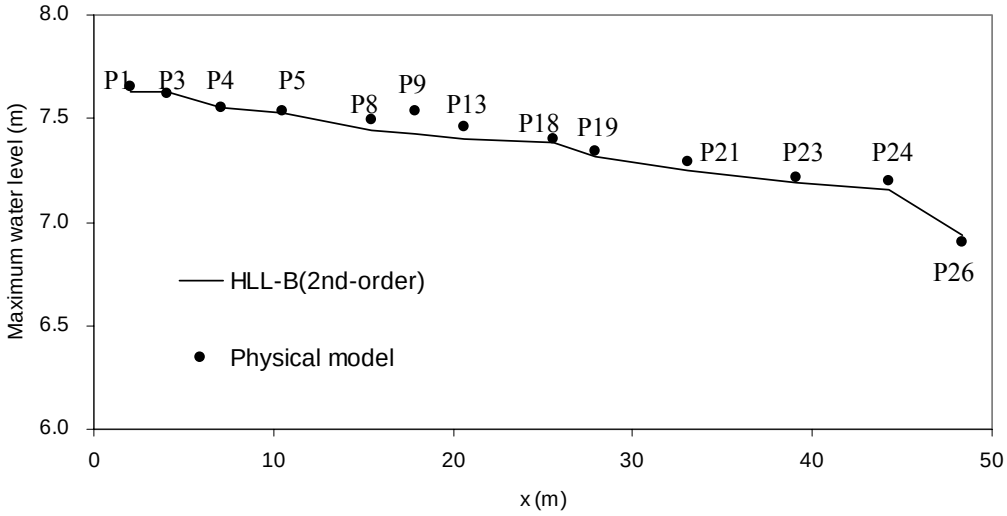

Fig. 14 Comparisons of maximum water level among numerical results and measured data for the Toce River test case

6. CONCLUSIONS

A new method has been proposed for implementing the approximate Riemann solvers for one-dimensional open channel flows. The method solves the form of the Saint Venant equations that include only one source term representing driving forces and use water surface level as one of primitive variables, in place of cross-sectional area. In addition, in the new method the discharge is evaluated according to the HLL flux, in stead of calculating it traditionally by solving the momentum equation. From both theoretical analysis and the results of several well-selected test examples, it has been clearly shown that the resulting scheme (HLL-B scheme) has excellent numerical balance and mass conservation property. The comparisons of computed results with analytical solutions and experimental data further demonstrate the ability of the HLL-B scheme to correctly depict the one-dimensional open channel flows that may include discontinuities, transcritical flows, wave interactions, and flows with irregular geometry and initial dry bed. The scheme's robustness and applicability to real-life open channel flows with complicated geometry are also well illustrated by means of test examples. It is important to note that this newly proposed method for implementing the approximate Riemann solvers should be also applicable to rectangular grid based two-dimensional shallow water flow simulations.

ACKNOWLEDGMENTS

This work is a result of research sponsored by the USDA Agriculture Research Service under Specific Research Agreement No. 58-6408-2-0062 (monitored by the USDA-ARS National Sedimentation Laboratory) and the University of Mississippi.

The authors are very grateful to Dr. Sandra Soares Frazao (University Catholique de Louvain) for her help in providing data set for the model validation in this paper.

REFERENCES

Cunge, J.A., Holly, F.M. Jr. and Verwey, A. (1980). *Practical Aspects of Computational River Hydraulics*, Pitman Publishing Limited, London.

Delis, A.I. (2002). "Higher Order Numerical Methods Evaluation for the Computation of One Dimensional Free Surface Shallow Water Flows". *International J. of Comput. Engrg. Science* 3(1), 13-55.

Delis, A. I. (2003). "Improved Application of the HLLE Riemann Solver for the Shallow Water Equations with Source Terms". *Commun. Numer. Meth. Engrg.* 19, 59-83.

Garcia-Navarro, P. and Vazquez-Cendon, M.E. (2000). "On Numerical Treatment of the Source Terms in the Shallow Water Equations". *Computers & Fluids* 29, 951-979.

Gharangik, A.M. and Chaudhry, M.H. (1991). "Numerical Simulation of Hydraulic Jump". *J. Hydraul. Engrg.* 117(9), 1195-1211.

Godunov, S.K. (1959). "Finite Difference Method for Numerical Computation of Discontinuous Solutions of the Equations of Fluid Dynamics". *Math. Sbonik* 47(3), 271-306 (in Russian).

Graf, W. H. and Altinakar, M. S. (1998). *Fluvial Hydraulics*, John Wiley & Sons Ltd, England.

Harten, A., Lax, P.D., and Van Leer, B. (1983). "On Upstream Differencing and Godunov-type Schemes for Hyperbolic Conservation Laws". *SIAM Review* 25(1), 35-61.

Hubbard, M and Garcia-Navarro, P. (2000). "Flux Difference Splitting and the Balancing of Source Terms and Flux Gradients". *J. Comput. Phys.* 165, 89-25.

Nujic, M. (1995). "Efficient Implementation of Non-Oscillatory Schemes for the Computation of Free-Surface Flows". *J. of Hydraul. Res*. 33 (1), 100-111.

Rogers, B.D., Borthwick, A.G.L. and Taylor, P. H. (2003). "Mathematical Balancing of Flux Gradient and Source Terms Prior to Using Roe's Approximate Riemann Solver". *J. Comput. Phys*. 192, 422-451.

Rosu, C. and Ahmed, M. (1999). "Toce River Dam-Break Test Case – A Comparison Between the ISIS Numerical Model and the Physical Model". *Proceedings of the 3rd CADAM workshop*, Milan, Italy.

Sanders, B.F. (2001). "High-Resolution and Non-Oscillatory Solution of the St. Venant Equations in Non-Rectangular and Non-Prismatic Channels". *J. of Hydraul. Res.* 39(3), 321-330.

Soares Frazao, S., Morris, M. and Zech, Y. (2000). *CADAM Project CD-ROM*, Produced by Hydraulics Division, Civil Engrg. Dept., Univ. Catholique de Louvain, Belgium.

Soares Frazao, S. and Zech, Y. (1999). "Computation of Extreme Flood Flow Through the Toce Valley". *Proceedings of the 3rd CADAM workshop*, Milan, Italy.

Toro, E.F. (2001). *Shock-Capturing Methods for Free-Surface Shallow Flows*. John Wiley & Sons Ltd.

Valiani, A., Caleffi, V. and Zanni, A. (2002). "Case Study: Malpasset Dam-Break Simulation Using a Two-Dimensional Finite Volume Method". *J. Hydraul. Engrg.* 128(5) 460-472.

Vazquez-Cendon, M. E. (1999). "Improved Treatment of Source Terms in Upwind Schemes for Shallow Water Equations in Channels with Irregular Geometry". *J. Comput. Phys.* 148, 497-526.

Ying, X., Khan, A. and Wang, S.S.Y. (2004). "Upwind Conservative Scheme for the Saint Venant Equation". *J. Hydraul. Engrg.* 130(10), 977-987.

Zhou, J.G., Causon, D.M., Mingham, C.G. and Ingram, D.M. (2001). "The Surface Gradient Method for the Treatment of Source Terms in the Shallow-Water Equations". *J. Comput. Phys.* 168, 1-25.

Zoppou, C. and Roberts, S. (2003). "Explicit Schemes for Dam-Break Simulations". *J. Hydraul. Engrg.* 129(1), 11-34.